J Therm Anal Calorim (2009) 98:401–408
DOI 10.1007/s10973-009-0304-0

Thermal decomposition reaction kinetics of complexes of $[Sm(o\text{-}MOBA)_3bipy]_2{\cdot}H_2O$ and $[Sm(m\text{-}MOBA)_3bipy]_2{\cdot}H_2O$

H. Y. Zhang · N. Ren · L. Tian · J. J. Zhang

Received: 25 November 2008 / Accepted: 6 January 2009 / Published online: 28 July 2009

Abstract The complexes of $[Sm(o\text{-}MOBA)_3bipy]_2{\cdot}H_2O$ and $[Sm(m\text{-}MOBA)_3bipy]_2{\cdot}H_2O$ ($o(m)$-MOBA = $o(m)$-methoxybenzoic acid, bipy-2,2′-bipyridine) have been synthesized and characterized by elemental analysis, IR, UV, XRD and molar conductance, respectively. The thermal decomposition processes of the two complexes were studied by means of TG–DTG and IR techniques. The thermal decomposition kinetics of them were investigated from analysis of the TG and DTG curves by jointly using advanced double equal-double steps method and Starink method. The kinetic parameters (activation energy E and pre-exponential factor A) and thermodynamic parameters ($\Delta H^{\neq}$, $\Delta G^{\neq}$ and $\Delta S^{\neq}$) of the second-step decomposition process for the two complexes were obtained, respectively.

Keywords 2, 2′-Bipyridine · o-Methoxybenzoic acid · m-Methoxybenzoic acid · Thermal decomposition mechanism · Non-isothermal kinetics · Samarium(III) complexes

H. Y. Zhang · L. Tian · J. J. Zhang (✉)
Experimental Center, Hebei Normal University, Shijiazhuang 050016, People's Republic of China
e-mail: jjzhang6@126.com

H. Y. Zhang · L. Tian
College of Chemistry and Material Science, Hebei Normal University, Shijiazhuang 050016, People's Republic of China

N. Ren
Department of Chemistry, Handan College, Handan 056005, People's Republic of China

Introduction

There has been a large body of research on the coordination of trivalent lanthanide cations with various carboxylic acids in recent years [1–9], due to their variety of structural types and potential applications in different interesting areas. Specially, lanthanide complexes with benzoic acid and its derivatives show fascinating crystal structures because of the variable coordination number of center metal as well as coordination versatility of carboxylic ligands. Concerning the kinetics and thermal decomposition mechanism of the rare earth carboxylate coordination complexes, which have been extensively studied in our literatures [10–17]. As a continuation of investigations in this area, we report herein the preparation and characterization of the two new complexes formed via the reaction of methoxybenzoic acid with different substitution position and 2,2′-bipyridine as co-ligands with Sm(III) ion. Meanwhile, thermal decomposition mechanism of these complexes are determined by TG–DTG and IR techniques, and the corresponding non-isothermal kinetics are discussed by advanced double equal-double steps method, together with Starink method [18]. The activation energy values obtained by the advanced double equal-double steps method based on iteration method is more exact than those obtained by double equal-double steps method [19] based on traditional isoconversional method.

Experimental

Materials

All the reagents used were AR grade without further purification.

Synthesis of the title complexes

A stoichiometric amount of $SmCl_3{\cdot}6H_2O$, L (L = *o*-HMOBA or *m*-HMOBA) and 2,2′-bipyridine were dissolved into 95% ethanol, respectively. The pH value of L solution was adjusted to 6–7 with 1.0 mol L^{-1} NaOH solution. The ethanolic solution of the two ligands was mixed and then added slowly to the $SmCl_3{\cdot}6H_2O$ solution with continuous stirring for 3 h. After the precipitates were isolated by filtration and then dried and stored with the yield of 50 and 77%, respectively.

Apparatus and conditions of experiment

Analysis of C, H, and N were determined by elemental analysis on a Vario-EL III elemental analyzer, while metal contents were obtained by using EDTA titration method with xylenol orange (XO) as an indicator. Infrared spectroscopy was recorded at room temperature in the frequency range of 4,000–400 cm^{-1} on a Bio-Rad FTS-135 spectrometer using the KBr discs. The ultraviolet spectroscopy was recorded on a Shimadzu 2501 spectrophotometer over the wavelength 250–400 nm range. XRD identification was carried out for the crystalline analyses on a Bruker D8-ADVANCE X-ray diffractometer in a scanning of 5–50° (2θ) with Cu Kα radiation ($\lambda = 250$ nm). The molar conductance was determined by a DDS-307 conductometer that was made in Shanghai exactitude apparatus factory. The TG–DTG curves of the two title complexes were obtained under static air atmosphere with a Perkin-Elmer TGA7 thermogravimetric analyzer. The heating rates were 3, 5, 7, 10 K·min^{-1} and the sample masses were 2.8–3.2 mg, respectively.

Methodology and kinetic analysis

Determination of the function of conversion

The equations of iteration calculation in an accurate kinetic study [20] are as follows:

$$\ln\frac{\beta}{H(x)} = \left\{\ln\left[\frac{0.0048\,AE}{R}\right] - \ln G(\alpha)\right\} - 1.0516\frac{E}{RT} \quad (1)$$

$$\ln\frac{\beta}{h(x)T^2} = \left[\ln\left(\frac{AR}{E}\right) - \ln G(\alpha)\right] - \frac{E}{RT} \quad (2)$$

thereinto: $H(x) = \dfrac{\exp(-x)}{0.0048\exp(-1.0516x)}h(x)$

$$h(x) = \frac{x^4 + 18x^3 + 86x^2 + 96x}{x^4 + 20x^3 + 120x^2 + 240x + 120}$$

Equations 1 and 2 are changed into:

$$\ln G(\alpha) = \ln\left(\frac{0.0048AEH(x)}{R}\right) - 1.0516\frac{E}{RT} - \ln\beta \quad (3)$$

$$\ln G(\alpha) = \ln\left(\frac{ARh(x)}{E}T^2\right) - \ln\beta \quad (4)$$

Where $G(\alpha)$ is the integral mechanism function, T(K) the absolute temperature, A(min^{-1}) the pre-exponential factor, R(8.314 J mol^{-1} K^{-1}) the gas constant, E(kJ mol^{-1}) the apparent activation energy and β(K min^{-1}) the linear heating rate. On substitution the values of conversion degrees at the same temperature on several TG curves, the different mechanism functions $G(\alpha)$ [21] and various heating rates into Eq. 3 or Eq. 4, the linear correlation coefficient r, the slope b and the intercept a at different temperatures were obtained by the linear least squares method with $\ln G(\alpha)$ versus $\ln\beta$. The corresponding function is the probable mechanism function of a solid phase reaction, if the linear correlation coefficient r is the best while the slope b approaches −1.

The calculation of E and A with the iteration method

The activation energy calculated by plots of $\ln\beta$ versus $1/T$ or $\ln(\beta/T^2)$ versus $1/T$ based on the traditional isoconversional method is not exact, as the traditional isoconversional method neglects the variation of $H(x)$ or $h(x)$ against x. However, iterative calculations by considering the change in $H(x)$ and $h(x)$ by means of plots of $\ln(\beta/H)$ versus $1/T$ or $\ln(\beta/hT^2)$ versus $1/T$ can give the exact value of activation energy, no matter how little or great the E/RT value of the reaction is.

The steps of E calculated by the iteration method [20] are as follows:

Step 1: Supposing $H(x) = 1$ or $h(x) = 1$ to estimate the initial value of the activation energy E_1.

Step 2: Calculate $H(x)$ or $h(x)$ using E_1, then calculate a new value E_2 from Eq. 1 or Eq. 2 via the plot of $\ln(\beta/H)$ versus $1/T$ or $\ln(\beta/hT^2)$ versus $1/T$.

Step 3: Repeat step 2, replacing E_1 with E_2, and so on, until the absolute difference of $(E_i - E_{i-1})$ is less than a defined small quantity such as 0.1 kJ mol^{-1}. The last value E_i is the exact value of the activation energy of the reaction. If the reaction mechanism is known, the exact pre-exponential factor A can be calculated from the intercept of the plot at the same time.

Starink method for determining E.

$$\ln\left(\frac{\beta}{T_f^{1.8}}\right) = -A\frac{E_a}{k_B T_f} + \text{constant} \quad (5)$$

Where $A = 1.0070 - 1.2 \times 10^{-5}E_a$ (kJ mol^{-1}), β is the heating rate and T is the temperature at a fixed amount transformed. It is based on the slope of a logarithmic function containing the heating rate versus l/T.

Results and discussion

Elemental analysis and molar conductance

The contents of C, H, N and Sm of the two complexes are shown in Table 1. The experimental data are in a good accord with the theoretical values.

The two title complexes are colorless and stable at room temperature in air. And they are soluble in DMSO and DMF, however, insoluble in water, ethanol and acetone solution. The molar conductance are determined in DMSO solution with DMSO as a reference (as shown in Table 1). It can be concluded that the two complexes act as non-electrolyte [22].

Infrared spectra

Frequencies of characteristic absorption bands in IR spectra (cm^{-1}) for ligands and the complexes are shown in Table 2. The shift of $\nu_{C=N}$ (1,578 cm^{-1}) and δ_{C-H} (992,757 cm^{-1}) of bipy ligand to higher strong absorption bands of the two complexes, respectively, can be ascribed to the blockage of respiration vibration and raising energy caused by the two nitrogen atoms coordinating to metal ion, indicating the coordination of the nitrogen atoms of bipy ligand to Sm^{3+} ion [23]. The presence of the $\nu_{(Sm-O)}$ absorption bands, the appearance of $\nu_{as(COO-)}$ and $\nu_{s(COO-)}$ absorption bands for the two complexes and the disappearance of $\nu_{C=O}$ absorption bands for the two acid ligands may suggest the coordination of the oxygen atoms in carboxylic groups to Sm(III) ion [24]. The broad band at 3,446 cm^{-1} of the two title complexes are attributed to ν_{O-H} of water molecules.

Table 3 UV absorption of ligands and complexes in DMSO (λ:nm, A_{max})

Sample	λ:nm	A_{max}
bipy	280	0.28
o-HMOBA	262	0.02
m-HMOBA	260	0.04
[Sm(*o*-MOBA)$_3$bipy]$_2$·H$_2$O	282	0.48
[Sm(*m*-MOBA)$_3$bipy]$_2$·H$_2$O	282	0.43

Ultraviolet spectra

The UV absorption spectra of the ligands and complexes in DMSO are determined, and the maximum absorption wavelengths and molar absorption coefficients are given in Table 3. The absorption bands of the two complexes shift to longer wavelength compared with that of corresponding ligands, which are attributed to expansion of π-conjugated system caused by the metal coordination [25].

XRD

The results of the X-ray power diffraction for the ligands and complexes are shown in Fig. 1, suggesting that: (1) X-ray power diffraction of the two complexes are different from the corresponding ligands. (2) The complexes are not simple lap joint of the free bipy ligand and acid ligands. (3) The new phase, i.e., the two title complexes are formed.

Table 1 Data of elementary analysis and molar conductivity for the two title complexes

Complexes	Theoretical values				Experimental values				Λ/S cm^2 mol^{-1}
	Sm	C	H	N	Sm	C	H	N	
[Sm(*o*-MOBA)$_3$bipy]$_2$·H$_2$O	19.55	53.11	3.93	3.64	19.60	52.85	3.70	3.68	23.5
[Sm(*m*-MOBA)$_3$bipy]$_2$·H$_2$O	19.55	53.11	3.93	3.64	19.61	53.22	3.15	3.43	8.4

Table 2 IR absorption for ligands and complexes (cm^{-1})

Ligands and complexes	$\nu_{C=N}$	δ_{C-H}	$\nu_{C=O}$	$\nu_{as(COO-)}$	$\nu_{s(COO-)}$	$\triangle\nu$	ν_{RE-O}
bipy	1,578	992,757	–	–	–	–	–
o-HMOBA	–	–	1,695	–	–	–	–
m-HMOBA	–	–	1,694	–	–	–	–
[Sm(*o*-MOBA)$_3$bipy]$_2$·H$_2$O	1,592	1,011,759	–	1,592	1,407	185	416
[Sm(*m*-MOBA)$_3$bipy]$_2$·H$_2$O	1,597	996,766	–	1,578	1,402	176	418

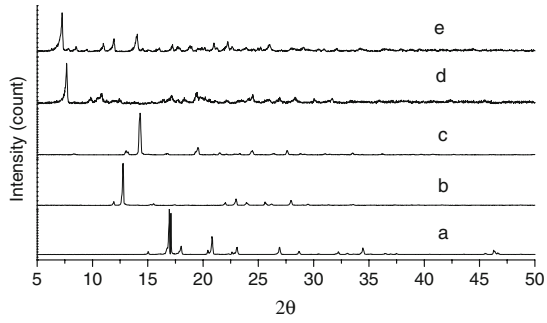

Fig. 1 XRD patterns of the complexes and the ligands. (a: bipy; b: *o*-HMOBA; c: *m*-HMOBA; d: $[Sm(o\text{-}MOBA)_3bipy]_2{\cdot}H_2O$; e: $[Sm(m\text{-}MOBA)_3bipy]_2{\cdot}H_2O$)

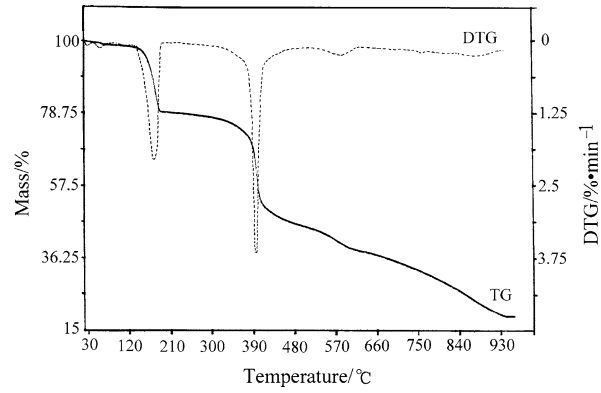

Fig. 3 The TG–DTG curves of the complex $[Sm(m\text{-}MOBA)_3bipy]_2{\cdot}H_2O$ at a heating of 3 K min^{-1}

Thermal decomposition mechanism

The thermal decomposition profiles of the two complexes are shown in Figs. 2 and 3, respectively. The TG–DTG curves show a continuous mass loss from room temperature to 1,223.15 K corresponding to several breaks indicating the formation of several intermediates. The thermal decomposition process of the complex $[Sm(o\text{-}MOBA)_3bipy]_2{\cdot}H_2O$ can be divided into multiple stages as shown in the DTG curves, and the thermal decomposition process of the complex $[Sm(m\text{-}MOBA)_3bipy]_2{\cdot}H_2O$ can be divided into four stages. The first mass loss observed between 298.15 and 374.5 K is due to dehydration with loss of H_2O (calcd. = 1.17%, TG = 0.83%) for the complex $[Sm(o\text{-}MOBA)_3bipy]_2{\cdot}H_2O$. And the first mass loss for the complex $[Sm(m\text{-}MOBA)_3bipy]_2{\cdot}H_2O$ between 298.15 and 377.40 K, corresponding to the release of one water molecule (calcd. = 1.17%, TG = 1.52%). After dehydration, the second-step thermal decomposition occurs from 374.5 to 466.03 K with the mass loss of 20.02% for the complex $[Sm(o\text{-}MOBA)_3bipy]_2{\cdot}H_2O$ and from 377.4 to 511.06 K with mass loss of 20.20% for the complex $[Sm(m\text{-}MOBA)_3bipy]_2{\cdot}H_2O$, corresponding to the loss of 2 bipy

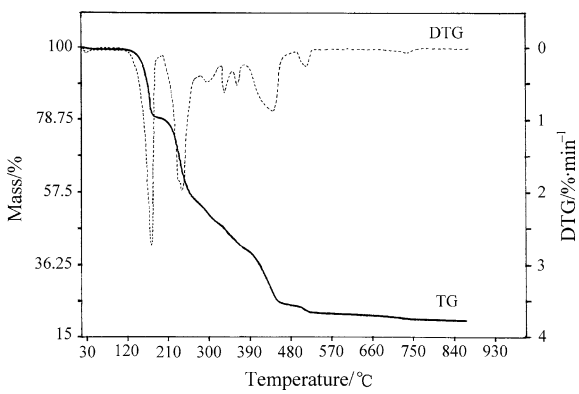

Fig. 2 The TG–DTG curves of the complex $[Sm(o\text{-}MOBA)_3bipy]_2{\cdot}H_2O$ at a heating of 3 K min^{-1}

with the theoretical mass loss of 20.31%. The IR spectra of the two residues at 466.03 and 511.06 K show the absorption bands of $\nu_{C=N}$ disappears at 1,592 cm^{-1}, 1,597 cm^{-1}, respectively. The final stages starts from 466.03 to 801.61 K for the complex $[Sm(o\text{-}MOBA)_3bipy]_2{\cdot}H_2O$, from 511.06 to 1,156.09 K for the complex $[Sm(m\text{-}MOBA)_3bipy]_2{\cdot}H_2O$, corresponding to the loss of acid ligands molecules. The total mass loss up to 801.61 K and 1,156.09 K for the two complexes are in excellent agreement with the formation of Sm_2O_3 as final residue (calcd. = 77.32%, 77.32%; TG = 77.15%, 77.10%), respectively. As seen in the IR spectra of the residue at 801.60 K for complex $[Sm(o\text{-}MOBA)_3bipy]_2{\cdot}H_2O$ and 1,156.09 K for complex $[Sm(m\text{-}MOBA)_3bipy]_2{\cdot}H_2O$, the asymmetric vibrations bands $\nu_{as(COO)}$ at 1,592 cm^{-1} and 1,631 cm^{-1} and the symmetric vibrations bands $\nu_{s(COO)}$ at 1,407 cm^{-1} and 1,402 cm^{-1} disappeared, respectively. The bands of the residue are both similar to the standard sample spectrum of Sm_2O_3. Based on the above analysis, the thermal decomposition processes of the two complexes can be expressed in the following ways:

$$\begin{aligned}\left[Sm(o\text{-}MOBA)_3bipy\right]_2{\cdot}H_2O &\rightarrow \left[Sm(o\text{-}MOBA)_3bipy\right]_2\\ &\rightarrow [Sm(o\text{-}MOBA)_3]_2\\ &\rightarrow Sm_2O_3\end{aligned}$$

$$\begin{aligned}\left[Sm(m\text{-}MOBA)_3bipy\right]_2{\cdot}H_2O &\rightarrow \left[Sm(m\text{-}MOBA)_3bipy\right]_2\\ &\rightarrow [Sm(m\text{-}MOBA)_3]_2\\ &\rightarrow Sm_2O_3\end{aligned}$$

From the initial decomposition temperature of the bipy ligand, it can be clearly seen that the two complexes are both quite heat stable. The order of thermal stability of the two complexes is as follows, which depends on the different substituted position.

$$\left[Sm(m-MOBA)_3bipy\right]_2{\cdot}H_2O > \left[Sm(o-MOBA)_3bipy\right]_2{\cdot}H_2O$$

Table 4 Conversion degrees measured for given the same temperatures on four TG–DTG curves of [Sm(o-MOBA)$_3$bipy]$_2$·H$_2$O at different heating rates (stage II)

T(K)	α			
	$\beta = 3$ K min^{-1}	$\beta = 5$ K min^{-1}	$\beta = 7$ K min^{-1}	$\beta = 10$ K min^{-1}
427.22	0.2397	0.1551	0.1000	0.07383
432.20	0.3514	0.2273	0.1500	0.1093
438.51	0.5456	0.3536	0.2500	0.1724
440.74	0.6346	0.4175	0.3000	0.2079
444.60	0.8159	0.5507	0.4000	0.2734

Table 5 Conversion degrees measured for given the same temperatures on four TG–DTG curves of [Sm(*m*-MOBA)$_3$bipy]$_2$·H$_2$O at different heating rates (stage II)

T(K)	α			
	$\beta = 3$ K min^{-1}	$\beta = 5$ K min^{-1}	$\beta = 7$ K min^{-1}	$\beta = 10$ K min^{-1}
455.47	0.2299	0.1277	0.1000	0.06874
465.21	0.4358	0.2610	0.2000	0.1407
468.29	0.5219	0.3224	0.2500	0.1782
473.52	0.6952	0.4517	0.3500	0.2592
477.77	0.8440	0.5825	0.4500	0.3382

Table 6 Partial results obtained by the linear least squares method at different temperatures for the second stage of the [Sm(*o*-MOBA)$_3$bipy]$_2$·H$_2$O

T(K)	Function No[a]	a	b	r
	14	−0.02637	−0.7215	−0.9968
427.22	**25**	**−0.1346**	**−1.0007**	**−0.9964**
	37	0.06024	−1.1688	−0.9969
	14	0.1157	−0.7440	−0.9980
432.20	**25**	**0.02518**	**−0.9876**	**−0.9974**
	37	0.3337	−1.2567	−0.9980
	14	0.3108	−0.7927	−0.9992
438.51	**25**	**0.2035**	**−0.9580**	**−0.9985**
	37	0.7680	−1.4606	−0.9994
	14	0.3888	−0.8114	−0.9998
440.74	**25**	**0.2542**	**−0.9264**	**−0.9983**
	37	0.9754	−1.5740	−0.9985
	14	0.5878	−0.9230	−0.9996
444.6	**25**	**0.3563**	**−0.9249**	**−0.9968**
	37	1.5825	−2.0507	−0.9936

Bold represents the values of the probable mechanism function

[a] The function No. is from Tables 6 to 10 in Ref. [21]

Table 7 Partial results obtained by the linear least squares method at different temperatures for the second stage of the [Sm(*m*-MOBA)$_3$bipy]$_2$·H$_2$O

T(K)	Function No[a]	a	b	r
	18	−0.1821	−2.1236	−0.9960
455.47	28	−0.7155	−1.0424	−0.9962
	31	**−0.4367**	**−1.0233**	**−0.9964**
	18	0.5348	−2.1858	−0.9980
465.21	28	0.2896	−1.0349	−0.9983
	31	**−0.1308**	**−1.0084**	**−0.9987**
	18	0.7513	−2.1797	−0.9978
468.29	28	−0.2667	−1.0691	−0.9986
	31	**−0.04960**	**−0.9821**	**−0.9987**
	18	1.2032	−2.2781	−0.9968
473.52	28	−0.1016	−1.0497	−0.9980
	31	**0.1038**	**−0.9660**	**−0.9989**
	18	1.6895	−2.5000	−0.9959
477.77	28	0.08501	−1.1067	−0.9979
	31	**0.2416**	**−0.9774**	**−0.9993**

Bold represents the values of the probable mechanism function

[a] The function No. is from Tables 6 to 10 in Ref. [21]

Kinetics of the second decomposition stage

The determination of f(α) and G(α)

The values of conversion degrees at the same temperature on four TG-DTG curves of the two complexes are shown in Tables 4 and 5, respectively.

By substituting the values of α, β in Tables 4 and 5 and various conversion functions $G(\alpha)$ [21] into Eq. 3 or Eq. 4, the linear correlation coefficient r, the slope b and the intercept a at the different temperatures were obtained by the linear least squares method with $\ln G(\alpha)$ versus $\ln\beta$. Partial results are shown in Tables 6 and 7.

From the Table 6, it can be clearly seen that the linear coefficients r of the function No. 25 is the best and the slope b approaches -1 at five different temperatures. So the probable mechanism function of the second decomposition stage for the complex [Sm(*o*-MOBA)$_3$bipy]$_2$·H$_2$O is $G(\alpha) = 1 - (1 - \alpha)^{1/1} - \alpha, f(\alpha) = 1$.

In a similar way, from Table 7, the conclusion can be drawn that the function No. 31 is the probable mechanism function for the complex $[Sm(m\text{-}MOBA)_3bipy]_2{\cdot}H_2O$, i.e., $G(\alpha) = 1 - (1 - \alpha)^{1/2}$, $f(\alpha) = 2(1–\alpha)^{1/2}$.

The calculation of E and A

The values of temperature for thermal decomposition at the same degree of conversion on several curves of the two complexes are presented in Tables 8 and 9, respectively. By substituting the values of α, β and T in Tables 8 and 9, and the corresponding mechanism function determined above into Eq. 1 or Eq. 2 via the linear least squares method with $\ln\beta/H(x)$ versus $1/T$ or $\ln(\beta/h(x)T^2)$ versus $1/T$, the activation energy E can be calculated from the value of the slope, and the pre-exponential factor A can also be calculated from the value of the intercept. Meanwhile, Starink method was also used to determine the activation energy E. Above results are listed in Tables 10 and 11, respectively.

The E values computed with iterative method are good agreement with that by Starink method.

The thermodynamic parameters of activation can be calculated from the equations [26, 27].

$$A\exp(-E/RT) = v\exp(-\triangle G^{\neq}/RT) \quad (6)$$

$$\Delta H^{\neq} = E - RT \quad (7)$$

$$\Delta G^{\neq} = \Delta H^{\neq} - T\Delta S^{\neq} \quad (8)$$

where $v(s^{-1})$ is the Einstein Vibration frequency, $v = k_B T/h$ (where k_B and h are Boltzmann and Planck constant respectively), $\Delta G^{\neq}$(kJ mol^{-1}) is the Gibbs free enthalpy of activation, $\Delta H^{\neq}$(kJ mol^{-1}) is the enthalpy of activation,

Table 8 Temperatures corresponding to the same degree of conversion at different heating rates for $[Sm(o\text{-}MOBA)_3bipy]_2{\cdot}H_2O$ (StageII)

α	T(K)			
	$\beta = 3$ K min^{-1}	$\beta = 5$ K min^{-1}	$\beta = 7$ K min^{-1}	$\beta = 10$ K min^{-1}
0.15	421.50	427.00	432.20	436.26
0.20	424.90	430.88	435.73	440.25
0.25	427.71	433.66	438.51	443.12
0.30	430.37	435.86	440.74	445.88
0.35	432.11	438.13	442.94	447.78
0.40	434.12	439.72	444.60	449.74
0.45	435.76	441.44	446.22	451.54
0.50	437.00	442.97	447.56	452.65
0.55	438.54	444.18	449.12	454.38
0.60	439.74	445.80	450.21	455.46
0.65	440.90	446.84	451.39	456.64
0.70	441.85	448.01	452.53	457.83
0.75	443.02	449.17	454.06	459.40
0.80	444.18	450.64	455.25	460.61

Table 9 Temperatures corresponding to the same degree of conversion at different heating rates for $[Sm(m\text{-}MOBA)_3bipy]_2{\cdot}H_2O$ (StageII)

α	T(K)			
	$\beta = 3$ K min^{-1}	$\beta = 5$ K min^{-1}	$\beta = 7$ K min^{-1}	$\beta = 10$ K min^{-1}
0.15	449.94	457.45	460.95	466.19
0.20	453.78	461.38	465.21	469.94
0.25	456.92	464.35	438.29	473.21
0.30	459.33	467.27	471.03	475.72
0.35	461.61	469.35	473.52	478.42
0.40	463.76	471.55	475.54	480.56
0.45	465.54	473.51	477.77	482.58
0.50	467.54	475.3	479.15	484.07
0.55	469.12	477.13	480.97	485.87
0.60	470.72	478.50	482.57	487.22
0.65	472.21	479.84	483.84	488.50
0.70	473.72	481.43	485.39	490.12
0.75	475.22	482.70	486.60	491.36
0.80	476.65	484.32	488.11	492.57

Table 10 The values of the kinetic parameters computed by the iterative method and the Starink method for [Sm(*o*-MOBA)$_3$bipy]$_2$·H$_2$O (StageII)

	ln(β/H(x)) vs. 1/T		ln(β/h(x)T^2) vs. 1/T		Starink
	A (10^{12}/min^{-1})	E (kJ mol^{-1})	A (10^{12}/min^{-1})	E (kJ mol^{-1})	E (kJ mol^{-1})
0.15	6.95	115.61	6.93	115.10	115.19
0.20	4.88	114.38	4.86	113.87	113.98
0.25	6.81	115.53	6.78	115.02	115.13
0.30	8.25	116.24	8.22	115.73	115.83
0.35	8.33	116.28	8.30	115.77	115.87
0.40	11.84	117.55	11.79	117.04	117.14
0.45	11.75	117.56	11.70	117.05	117.15
0.50	21.04	119.64	20.96	119.12	119.22
0.55	14.18	118.29	14.12	117.77	117.87
0.60	30.19	121.06	30.07	120.52	120.62
0.65	31.61	121.25	31.48	120.72	120.82
0.70	22.97	120.12	22.88	119.59	119.70
0.75	10.03	117.21	9.99	116.70	116.81
0.80	12.32	118.06	12.27	117.54	117.65
Average	14.37	117.77	14.31	117.25	117.36

Table 11 The values of the kinetic parameters computed by the iterative method and the Starink method for [Sm(*m*-MOBA)$_3$bipy]$_2$·H$_2$O (StageII)

	ln(β/H(x)) vs. 1/T		ln(β/h(x)T^2) vs. 1/T		Starink
	A (10^{12}/min^{-1})	E (kJ mol^{-1})	A (10^{12}/min^{-1})	E (kJ mol^{-1})	E (kJ mol^{-1})
0.15	3.64	123.79	3.62	123.25	123.35
0.20	6.07	125.68	6.05	125.12	125.22
0.25	7.86	126.62	7.83	126.06	126.17
0.30	8.21	126.77	8.18	126.22	126.32
0.35	4.89	124.81	4.87	124.26	124.37
0.40	7.38	126.39	7.36	125.84	125.94
0.45	4.99	124.91	4.97	124.36	124.47
0.50	22.18	130.64	22.10	130.07	130.17
0.55	16.88	129.62	16.81	129.05	129.16
0.60	29.39	131.76	29.27	131.18	131.28
0.65	64.47	134.80	64.21	134.21	134.31
0.70	64.64	134.87	64.38	134.27	134.37
0.75	151.17	138.19	150.56	137.58	137.69
0.80	268.53	140.48	267.47	139.86	139.95
Average	47.16	129.95	46.98	129.38	129.48

Table 12 The thermodynamic parameters of the two title complexes

Complexes	β (K min^{-1})	$\Delta H^{\neq}$ (kJ mol^{-1})	$\Delta G^{\neq}$ (kJ mol^{-1})	$\Delta S^{\neq}$ (J mol^{-1} K^{-1})	T_P (K)
[Sm(*o*-MOBA)$_3$ bipy]$_2$·H$_2$O	3	113.83	115.90	−4.68	442.78
	5	113.80	115.92	−4.74	445.68
	7	113.74	115.95	−4.87	453.01
	10	113.70	115.98	−4.98	458.78
	Average value	113.77	115.94	−4.82	
[Sm(*m*-MOBA)$_3$ bipy]$_2$·H$_2$O	3	125.72	123.52	4.63	474.74
	5	125.66	123.49	4.51	482.00
	7	125.63	123.47	4.43	486.44
	10	125.59	123.45	4.36	490.37
	Average value	125.65	123.48	4.48	

$\Delta S^{\neq}$(J mol^{-1} K^{-1}) is the entropy of activation. The values of entropy, enthalpy and the Gibbs free energy of activation at the peak temperature obtained on the basis of Eqs. 6–8 are listed in Table 12. The values of $\Delta G^{\neq} > 0$ for the two complexes indicate that their decomposition reaction are not spontaneous reactions.

Conclusions

The two samarium complexes of [Sm(*o*-MOBA)$_3$-phen]$_2$·H$_2$O and [Sm(*m*-MOBA)$_3$phen]$_2$·H$_2$O were synthesized. The mechanism function of the second-stage decomposition reaction of the two complexes are $G(\alpha) = 1 - (1 - \alpha)^{1/1} - \alpha$, $f(\alpha) = 1$ and $G(\alpha) = 1 - (1 - \alpha)^{1/2}$, $f(\alpha) = 2(1 - \alpha)^{1/2}$. The activation energy E are 117.51 kJ mol^{-1}, 129.66 kJ mol^{-1} and the pre-exponential factor A are 14.34×10^{12} min^{-1}, 47.07×10^{12} min^{-1}, respectively. The enthalpy of activation $\Delta H^{\neq}$, the Gibbs free energy of activation $\triangle G^{\neq}$ and the entropy of activation $\Delta S^{\neq}$ at the peak temperature were also obtained. Moreover, the values of $\Delta G^{\neq} > 0$ for the two complexes indicate that their decomposition reaction are not spontaneous reactions.

Acknowledgements This project was supported by the National Natural Science Foundation of China (No. 20773034), the Natural Science Foundation of Hebei Province (No. B2007000237) and Science Foundation of Hebei Normal University (No. L2006Z06).

References

1. Singh UP, Kumar R, Upreti S. Synthesis, structural, photophysical and thermal studies of benzoate bridged Sm(III) complexes. J Mol Struct. 2007;831:97–105.
2. Seward C, Hu NX, Wang S. 1-D Chain and 3-D grid green luminescent terbium(III) coordination polymers: {Tb(O_2CPh)$_3$(CH_3OH)$_2$(H_2O)}$_n$ and {Tb$_2$(O_2CPh)$_6$(4,4′-bipy)}$_n$. J Chem Soc Dalton Trans. 2001;134–7.
3. Lam AWH, Wang WT, Gao S, Wen GH, Zhang XX. Synthesis, crystal structure, and photophysical and magnetic properties of dimeric and polymeric lanthanide complexes with benzoic acid and its derivatives. Eur J Inorg Chem. 2003;2003:149–63.
4. Li Y, Zheng FK, Liu X, Zou WQ, Guo GC, Lu CZ, et al. Crystal structures and magnetic and luminescent properties of a series of homodinuclear lanthanide complexes with 4-cyanobenzoic ligand. Inorg Chem. 2006;45:6308–16.
5. Wan YH, Zhang LP, Jin LP, Gao S, Lu SZ. High-dimensional architectures from the self-assembly of lanthanide ions with benzenedicarboxylates and 1,10-phenanthroline. Inorg Chem. 2003;42:4985–94.
6. Li X, Zhang ZY, Zou YQ. Synthesis, structure and luminescence properties of four novel terbium 2-fluorobenzoate complexes. Eur J Inorg Chem. 2005;14:2909–18.
7. Li GQ, Li Y, Zou WQ, Chen QY, Zheng FK, Guo GC. Synthesis and crystal structure of a new lanthanum(III) 4-cyanobenzoate complex. Chin J Struct Chem. 2007;26:575–9.
8. Siqueira AB, Bannach G, Rodrigues EC, Carvalho CT, Ionashiro M. Solid-state 2-methoxybenzoates of light trivalent lanthanides. J Therm Anal Calorim. 2008;91(3):897–902.
9. Locatelli JR, Rodrigues EC, Siqueira AB, Ionashiro EY, Bannach G, Ionashiro M, et al. Synthesis, characterization and thermal behaviour of solid-state compounds of yttrium and lanthanide benzoates. J Therm Anal Calorim. 2007;90(3):737–46.
10. Ren N, Zhang JJ, Zhang CY, Xu SL, Zhang HY, Tian L. Thermal decomposition kinetics of Sm(III) complex with *o*-nitrobenzoate and 1,10-phenanthroline. Chin J Inorg Chem. 2007;23:1078–84.
11. Zhang JJ, Xu SL, Ren N, Zhang HY. Preparation, crystal structure and mechanism of thermal decomposition of complex [Dy(*p* -MOBA)$_3$Phen]$_2$. Russ J Coord Chem. 2007;33:611–5.
12. Zhang JJ, Ren N, Xu SL. Synthesis and thermal decomposition kinetics of the complex of xamarium *p*-methylbenzoate with 1,10-phenanthroline. Chin J Chem. 2007;25:125–8.
13. Zhang JJ, Ren N, Chai XQ, Wang YX. Non-isothermal kinetics of the first-stage decomposition reaction of the complex of samarium *p*-methoxybenzoate with 1,10-phenanthroline. Rare Metals. 2007;26:292–8.
14. Xu SL, Zhang JJ, Yang HF, Ren N, Zhang HY. Synthesis, crystal structure and thermal decomposition of a dysprosium(III) *p*-fluorobenzoate 1,10-phenanthroline complex. J Chem Sci. 2007;62b:51–4.
15. Zhang JJ, Ren N, Wang YX, Xu SL, Wang RF, Wang SP, et al. Synthesis, crystal structure and thermal decomposition mechanism of a samarium*o*-chlorobenzoate complex with 1,10-phenanthroline. J Braz Chem Soc. 2006;17(7):1355–9.
16. Zhang JJ, Wang RF, Liu HM, Li JB, Ren N. Non-isothermal kinrtics of the first stage decomposition reaction of the complex of terbium *t*-methylbenzoate with 1,10-phenanthroline. Chin J Chem. 2005;23:646–50.
17. Zhang JJ, Wang RF, Wang SP, Liu HM, Li JB, Bai JH, et al. Preparation, thermal decomposition process and kinetics for terbiump-methoxybenzoate ternary complex with 1,10-phenanthroline. J Therm Anal Calorim. 2005;79:181–6.
18. Starink MJ. A new method for the derivation of activation energies from experiments performed at constant heating rate. Thermochim Acta. 1996;288:97–104.
19. Zhang JJ, Ren N. A new kinetic method of processing TA data. Chin J Chem. 2004;22:1459–62.
20. Gao Z, Nakada M, Amasaki I. A consideration of errors and accuracy in the isoconversional methods. Thermochim Acta. 2001;369:137–42.
21. Hu RZ, Gao SL, Zhao FQ, Shi QZ, Zhang TL, Zhang JJ. Thermal analysis kinetics. 2nd ed. Beijing: Science Press; 2008. p. 151.
22. Geary WJ. The use of conductivity measurements in organic solvents for the characterisation of coordination compounds. Coord Chem Rev. 1971;7:81–122.
23. Wang RF, Jin LP, Wang MZ, Huang SH, Chen XT. Synthesis crystal structure and luminescence of coordination compound of europium *p*-methylbenzoate with 2,2́-dipyridine. Acta Chim Sinica. 1995;53(1):39–45.
24. Shi YZ, Sun XZ, Jiang YH. Spectra and chemical identification of organic compounds. Nanjing: Science and Technology Press; 1988. p. 98.
25. An BL, Gong ML, Li MX, Zhang JM. Synthesis, structure and luminescence properties of samarium (III) and dysprosium (III) complexes with a new tridentate organic ligand. J Mol Struct. 2004;687:1–6.
26. Straszko J, Olstak-Humienik M, Mozejko J. Kinetics of thermal decomposition of $ZnSO_4$·7H_2O. Thermochim Acta. 1997;292:145–50.
27. Olstak-Humienik M, Mozejko J. Thermodynamic functions of activated complexes created in thermal decomposition processes of sulphates. Thermochim Acta. 2000;344:73–9.